Green Chemistry

Accepted Manuscript

ROYAL SOCIETY OF CHEMISTRY

www.rsc.org/greenchem

Journal Name

RSCPublishing

ARTICLE

Molybdenum Incorporated Mesoporous Silica Catalyst for Production of Biofuels and Value-added Chemicals via Catalytic Fast Pyrolysis

Cite this: DOI: 10.1039/x0xx00000x

Received 00th January 2012,
Accepted 00th January 2012

DOI: 10.1039/x0xx00000x

www.rsc.org/

Sridhar Budhi,[a,b,] Calvin Mukarakate,[a,] Kristiina Iisa,[a] Svitlana Pylypenko,[b] Peter N. Ciesielski,[a] Matthew M Yung,[a] Bryon S. Donohoe,[a] Rui Katahira,[a] Mark R. Nimlos,[a] and Brian G. Trewyn[b*]*

Production of value-added furans and phenols from biomass through catalytic fast pyrolysis of pine using molybdenum supported on KIT-5 mesoporous silica support was explored. Catalysts containing different loadings of molybdenum were synthesized and characterized by X-ray diffraction, physisorption and chemisorption analysis, various electron microscopic techniques and X-ray photoelectron spectroscopy. Characterization studies indicate that molybdenum is homogeneously distributed over the KIT-5 silica support in a +6 oxidation state. Fast pyrolysis of pine using molecular beam mass spectrometry with fresh Mo catalyst preferentially produced furans and phenols over conventionally observed aromatic hydrocarbons. Detailed investigation of model biopolymers indicates that the furans originated from the carbohydrate portion of the biomass and the phenols emerged predominantly from the lignin portion of biomass. Results obtained from MBMS were complemented using pyrolytic-GCMS.

1. Introduction

With the discovery of fossil fuels two centuries ago, biomass has been replaced as the primary source of energy and chemicals mainly due to low cost and vast abundance of fossil fuels. However, rapid depletion of these natural resources and growing concerns about carbon dioxide emissions and national security has necessitated the global scientific community to turn its attention towards sustainable and renewable energy sources. Humans are utilizing only a tiny percentage of the 170 billion metric tons of biomass produced annually in nature through photosynthesis.[1, 2] One example of biomass is lignocellulosic material from terrestrial plants. Lignocellulosic biomass presents an abundant, alternate resource for the production of fuels and several value-added chemicals. The United States Department of Energy has released a list of top 10 platform chemicals, chemicals that can be used to synthesize many important molecules.[3] Furans are among the top ten chemicals that have great potential to meet our goals for renewable production of fuels and chemicals. They can serve as valuable precursors for production of fuels in the jet and diesel pool range[4] or as precursors in the synthesis of specialty polymers, agrochemical and pharmaceutical intermediates, cross-linking agents, fine chemicals and macrocyclic ligands.[5-7]

Furans are typically produced by dehydration reactions of carbohydrates. The conventional pathways used for selective

production of furans include: organic solvents, aqueous phase, multiphase solvent, and ionic liquid systems.[8-11] A wide range of catalytic based solvent systems were explored for the production of furans. Several homogeneous inorganic and organic acidic compounds were reported for selective production of furans from biomass or its components, typically carbohydrates. The acids that were identified as catalysts for production of furans were either Lewis acids or protic mineral acids such as HCl, H_2SO_4, and H_3PO_4.[9, 12] Examples of organic acids found to be active for carbohydrate dehydration is *p*-toluenesulfonic acid, oxalic acid and levulinic acid.

In addition to acids in solution, several examples of solid and multiphasic systems have been reported in the literature for production of furans through dehydration. All lanthanides were found to be active for production of furans but with different efficacies.[13] Halides of transition metals in 1-ethyl-3-methylimidazolium chloride and main group elements such as tin and aluminum were also found to be active for synthesis of furans.[11] Solid acid catalysts such as H-form zeolites, amberlyst-15, titania, and sulfated zirconia were investigated and found to be efficient for the production of furans.[14-17] Detailed discussion of the above mentioned catalysts and additional catalytic systems that have been explored for the production of furans have been reviewed recently.[18] Reports published for furan production from renewable resources are common in solution phase but no selective gas phase production has been reported to the best of our knowledge.

Growing concern for environmental sustainability has led researchers to find alternatives for homogeneous, environmentally hazardous catalysts. It is imperative to discover and employ heterogeneous catalysts for production of furans from biomass. Solid acids and recyclable ionic liquid containing catalysts have already been investigated for the synthesis of furans; however, the heterogeneous catalysts reported so far suffer from low surface areas, small pore diameters, and a lack of hydrothermal stability to tolerate the harsh pyrolytic reaction conditions. Furthermore, those catalysts offer limited opportunities to customize pore size and structure, morphology or hydrothermal stability for specific applications.

Mesoporous silica (periodic or aperiodic) has been widely investigated for application as catalyst supports.[19-22] Methods to tune pore size and structure, morphology, and the surface chemistry for mesoporous silica are well understood. Mesoporous silica supports with various pore structures have been widely reported in the literature.[23] Of the several pore morphologies, 3-dimensional pore structures (e.g., SBA-2, -6, -7, -16; KIT-5; IBN-1; FDU-1, -2, -12)[23] are of significant interest, as they have better mass transfer properties than the conventional 2D pore structures such as MCM-41, MCM-50 and SBA-15.[19, 24-26] For the reasons listed above, we chose KIT-5, which has the desired three-dimensional pore structure for this investigation.

Molybdenum has been extensively studied and is widely used in the petroleum industry for fuel upgrading reactions such as hydrodeoxygenation, hydrodenitrogenation and hydrodesulfurization.[27] Molybdenum was also investigated for alkane oxidation and ring opening of epoxides by alcohols and amines.[28] Interestingly, molybdenum has many properties parallel to those of noble metals, but is not as costly or scarce. Despite these advantages, the catalytic properties of molybdenum have not been explored for the production of furans or for use in catalytic fast pyrolysis reactions. Herein, we report the synthesis of molybdenum incorporated KIT-5 mesoporous silica catalysts for production of value-added furans through catalytic fast pyrolysis of lignocellulosic biomass.

2. Experimental Section

2.1.1 Materials: All materials used for the catalyst syntheses were purchased from Sigma-Aldrich and Fisher Scientific and used without further purification. Avicel cellulose was

purchased from Sigma-Aldrich and lignin was obtained from Asian Lignin Manufacturing.[29] Idaho National Laboratory supplied the southern yellow pine, which has approximately 42% cellulose, 21% hemicellulose and 30% lignin with the balance attributed to minerals and inorganic salts.[29]

2.1.2 Catalyst synthesis: The synthetic procedure adopted for the catalyst was based on the previously published report.[30] Neutral pluronic polymer surfactant F127 (4 g) was dissolved in 240 mL of nano-pure water, heated to 318 K and charged with 3.4 mL of concentrated hydrochloric acid. The reaction mixture was stirred for 1 h, and variable amounts of ammonium heptamolybdate tetrahydrate, the molybdenum precursor, were added to the solution. Tetraethylorthosilicate (24 g) was immediately added dropwise to the reaction mixture and allowed to stir continuously for 24 h. After 24 h, the container was transferred to an oven at 363 K and subjected to static hydrothermal treatment for another 24 h. The reaction mixture was hot-filtered and washed with 15 ml of nano-pure water. The collected precipitate was oven dried overnight at 358 K. The as-synthesized catalyst was calcined at 773 K for 8 h to remove the surfactant template. The synthesized catalysts are referred to as Xg-Mo, where Xg represents the amount of molybdenum precursor added in grams during the synthesis.

2.2 Catalyst characterization

2.2.1. X-ray diffraction analysis: The X-ray diffraction patterns were recorded using Rigaku Ultima IV diffractometer with Cu Kα radiation source with a step size of 0.02 degrees/sec. Low angle studies were performed to study the pore structure arrangement and wide angle studies were conducted to investigate the active species in the catalyst.

2.2.2 Textural properties analysis: A Micromeritics Tristar 3020 instrument was used to investigate the textural properties of the catalyst. The samples were degassed under flowing helium at 373 K for 5 h to remove impurities adsorbed on the surface of the catalyst. After degassing, the catalyst was subjected to nitrogen physisorption analysis to evaluate specific surface area, pore volume, pore size distribution, and pore diameter. The Brunauer-Emmett-Teller (BET) and Barrett-Joyner-Halenda (BJH) equations were used to calculate specific surface area and pore size distribution, respectively.

2.2.3 Scanning Electron Microscopy (SEM): SEM was performed using an FEI Quanta 400 FEG instrument. Samples were mounted on aluminum stubs with conductive carbon tape adhesive prior to imaging. Images were obtained at an accerlating voltage of 20 keV.

2.2.4 Energy Dispersive X-Ray Spectroscopy (EDS): EDS was performed in the aforementioned SEM instrument equipped with an EDAX X-ray detector using the same sample preparation methods used for SEM imaging. For each sample, elemental composition was obtained from at least 20 different particle agglomerates located at different regions on the mounting stub using automated particle analysis and spectrum aquisition. Spectra were quantified using an atomic number (ZAF) correction. EDS mapping was performed in Quant mode based on net intensity using a dwell time of 200 ms per pixel, using the same instrument and sample preparation techniques.

2.2.5 Transmission Electron Microscopy (TEM): Catalyst particles were suspended in ethanol and drop-cast onto carbon-coated, 200 mesh copper grids (SPI Supplies, West Chester, PA). Grids were allowed to air dry prior to imaging. Imaging was performed using an accelerating voltage of 200 keV, and images were captured with a four mega-pixel Gatan UltraScan 1000 camera (Gatan, Pleasanton, CA) on a FEI Tecnai G2 20 Twin 200 kV LaB6 TEM (FEI, Hilsboro, OR).

2.2.6 X-ray Photoelectron Spectroscopy (XPS): X-ray photoelectron spectra were measured on a Kratos Nova X-ray photoelectron spectrometer supplied with a

monochromatic Al Kα source operating at 300 W. Survey and high resolution C 1s, O 1s, Mo 3d and Si 2p spectra were acquired from at least three areas per sample. Quantification and processing were performed using Casa XPS software, utilizing manufacturer provided sensitivity factors. A linear background was applied to C 1s, O 1s, and Si 2p regions, and a Shirley background was applied to Mo 3d region. Spectra were charge referenced using Au $4f_{7/2}$ at 84 eV. After calibration, Si 2p spectrum was centered at 104.3 eV, typical binding energy for SiO_2 calibrated with gold.

2.2.7 Temperature Programmed Desorption of Ammonia (NH_3-TPD): NH_3-TPD measurements were performed using Micromeritics Autochem 2920 instrument to measure total surface acidity and acid strength of the catalysts. A U-shaped, flow through, micro quartz reactor containing ~100 mg of catalyst was activated at 773 K for 120 min under flowing He (50 ml min^{-1}) and cooled to 393 K before exposure to ammonia. Adsorption of ammonia was performed by flowing 10% NH_3/He for 30 min at 393 K followed by flushing with He to remove physisorbed ammonia. Ammonia desorption was recorded via thermal conductivity detector (TCD) by ramping the sample temperature from 393 K to 773 K at a rate of 30 K min^{-1}. Quantification of amount of ammonia desorbed from the samples was done using a sample loop of known volume to calibrate the TCD response for ammonia.

2.2.8 Pyridine DRIFTS: Pyridine DRIFTS experiments were conducted to determine the ratio of Lewis and Brønsted acid sites. In these experiments a Thermo FTIR with an MCT detector and Praying Mantis DRIFTS attachment were utilized. Catalyst samples were pretreated by heating in 100 sccm from 25-500°C at a ramp rate of 20 °C min^{-1} and held for 15 minutes and then cooled at a ramp rate of 20 °C min^{-1} to 150 °C. Pyridine was adsorbed by flowing 100 sccm through a pyridine bubbler and then over the catalyst for 10 min. The sample was then flushed with at least 10 min prior to acquiring a spectrum at 150°C. The areas of peaks at 1545 cm^{-1} and 1455 cm^{-1}, corresponding to pyridine adsorbed on Brønsted and Lewis acid sites, respectively, were used to determine the relative concentrations of the types of acid sites, which were converted to absolute concentrations of acid sites by using the total acidity as determined by ammonia TPD. That ratio of the molar extinction coefficients (units cm μmol^{-1}) for Brønsted to Lewis acid sites was B/L = 0.75.[31, 32]

2.2.9 Thermogravimetric Analysis (TGA): Coke deposited on catalyst samples was quantified by TGA. TGA Instruments Q500 analyser was used to burn off the coke in the catalyst. The spent catalyst was heated in air at a ramp rate of 20 ^oC min^{-1} from 25 ^oC to 850 ^oC. The mass decrease below 250 ^oC was attributed to the loss of water and weakly adsorbed organic species and mass loss at the temperatures between 250 ^oC and 780 ^oC was attributed to carbonaceous coke.

2.3 Catalytic Fast Pyrolysis:

2.3.1 Horizontal reactor – MBMS: Fast pyrolysis of pine, lignin and cellulose were performed in a horizontal quartz annular flow reactor coupled to molecular beam mass spectrometer (MBMS).[29, 33-36] Batch-wise pyrolysis and vapor upgrading were performed using a reactor heated to 500 ^oC and a five-zone furnace. Quartz pulses containing 50 mg of biomass or its components were introduced into the inner tube of the reactor maintained at 500 ^oC. The pyrolysis vapors were carried by 0.2 standard liters per minute (slm) flow of helium through a fixed bed of catalyst (500 mg) supported on quartz wool. The flow in the inner tube was subsequently mixed with a 4 slm helium flow from the outer tube towards the end of the reactor prior to sampling by MBMS orifice. The MBMS is used for real-time sampling of pyrolysis products. Dilution of upgraded pyrolysis vapors by outer flow

of helium was necessary to minimize secondary reactions and to meet the flow demands of the sampling orifice. The upgraded pyrolysis vapors undergo adiabatic expansion through a 250 μm orifice into a vacuum chamber held at 100 mtorr and skimmed into a molecular beam, where it is ionized by electron impact ionization source (22.5 eV) producing positive ions that were measured using a quadrupole mass spectrometer. Mass spectra were collected every second over the m/z range of 10-450. Argon gas (40 sccm) mixed with helium carrier gas was used as a tracer gas to correct the drifts in signal due to changes in flow through the molecular beam inlet. Biomass, or its components, was fed batch-wise in a quartz pulse as 50 mg samples with a weight hourly space velocity of 3.6 hr^{-1} until the catalyst was deactivated.[29, 36]

2.3.2 Tandem micropyrolyzer-GCMS (py-GCMS): The results obtained from py-MBMS were complemented by py-GCMS for quantification of pyrolysis products. The py-GCMS was coupled to a tandem micropyrolyzer **(**Rx-3050TR, Frontier Laboratories, Japan) equipped with an autosampler (AS-1020E) and a microjet cryo-trap (MJT-1030Ex).[36] The micropyrolyzer has two heating zones: one for conducting pyrolysis and one for upgrading the pyrolysis vapors. Deactivated stainless cups containing 500 μg biomass (pine) were loaded into autosampler. The cups were automatically dropped into the pyrolysis zone maintained at 500 °C and the pyrolyzed vapors pass through the fixed catalyst bed (at 500 °C) for upgrading. The upgraded vapors were subsequently captured using a liquid nitrogen trap (-196 ^{o}C, housed inside the GC oven) and desorbed into the inlet of the gas chromatograph (7890B, Agilent Technologies, USA) interfaced with the MS (5977A, Agilent Technologies, USA). The trapped gases were separated by a capillary column (Ultra Alloy-5, Frontier Laboratories, Japan) with a 5 % diphenyl and 95 % dimethylpolysiloxane stationary phase. The oven was programmed to hold at 40 ^{o}C for 3 min followed by heating to 280 ^{o}C at the ramp rate of 10 ^{o}C min^{-1}. The separated pyrolysis vapors were identified using standards and NIST GCMS library.

2.3.3 Multivariate Analysis of MBMS Spectra: Multivariate analysis was utilized to identify groups of correlated mass spectral peaks in the product vapors and to track patterns of change as the catalyst deactivated. The multivariate curve resolution optimized by alternate least squares (MCR-ALS) found in the software package "The Unscrambler" (Camo Software AS, version 9.7) was used for analyzing complex mass spectra. Multivariate curve resolution (MCR) resolves the principal component analysis results into mathematically constructed components, which have mathematically derived sub-spectra that are used to partition the original variance of the data set into the estimates of the concentrations of the components.[37] This facilitates the determination of elution profiles of the components in an unresolved mixture of two or more constituents, assuming the data has enough degrees of freedom to identify the separate sources of variance. This is particularly useful because the mixtures encountered in this work are unavailable as pure components (PCs). The unscrambler MCR algorithm is based on pure-variable selection from principal component analysis (PCA) loadings to find the initial estimation of spectral profiles, and then alternating least squares to optimize resolved spectral concentration profiles. Constraints were introduced for generation of non-negative concentration profiles and mass-spectra. To represent the data accurately, constraints for unimodality and equality in concentration profiles were not included to account for variation of relative concentrations for pure components with biomass-to-catalyst ratio.

3. Results and Discussion

3.1.1 X-ray Diffraction Analysis: Three catalysts, 0.25g-Mo, 1g-Mo and 2g-Mo, with molybdenum weight loadings 1.5, 2.5, and 3.7 wt %, respectively, were synthesized. The molybdenum weight percent in the catalysts was measured by ICP-AES analysis (Table 1). The synthesized catalysts were subjected to low-angle X-ray diffraction measurements to determine the pore structure of Mo-modified KIT-5. The most

intense (111) peak corresponding to *Fm3m* symmetry for face-centered cubic pore structure was observed in all the three catalysts. However, higher order diffractions such as (200) and (220) were not clearly observed. The absence of higher order peaks is typical for metal-containing mesoporous silica materials synthesized by the co-condensation method.[28]

Table 1. Textural properties of catalysts containing different molybdenum loadings.

Catalyst	Specific Surface Area (m^2g^{-1})	Pore Volume (cm^3g^{-1})	Pore Diameter (nm)	Molybdenum (wt%) (ICP-AES)
0.25g-Mo	732	0.47	6.2	1.5
1g-Mo	690	0.47	5.6	2.5
2g-Mo	685	0.31	4.3	3.7

Representative X-ray diffraction spectra for the catalysts are shown Figure 1(a). Furthermore, the catalysts were subjected to wide-angle X-ray diffraction to characterize the nature of molybdenum species in the catalyst. X-ray diffraction spectra of 0.25g-Mo catalyst, pure silica KIT-5, commercially available molybdenum trioxide and ammonium molybdate are presented in Figure 1(b).

Commercial molybdenum trioxide and ammonium molybdate show characteristic peaks previously reported in the literature;[28, 38] however, sharp diffraction peaks corresponding to commercial molybdenum trioxide and ammonium molybdate were not observed in spectra for 0.25g-Mo catalyst. The diffraction pattern of this catalyst was very similar to pure silica KIT-5, indicating the molybdenum is uniformly dispersed in the silica matrix and the Mo loadings were too small for its crystal patterns to be detected by X-rays. Because the nature of the active catalyst could not be determined by wide-angle X-ray diffraction, XPS analysis was used to gain information on the state of the Mo species.

3.1.2 X-ray Photoelectron Spectroscopy (XPS) Analysis: A representative Mo 3d spectrum acquired from 2g-Mo sample is shown in Figure 2. The $3d_{5/2}$ component is located at 233.6 eV, at the higher end of the binding energies reported for Mo(VI) oxides.[39-41] Comparing Mo 3d spectrum acquired from the 2g-Mo sample with that of the reference MoO_3 located at 232.6 eV[42] it becomes evident that the majority of the molybdenum species in the synthesized material have higher binding energies (BE) than the molybdenum in the reference MoO_3. The spectrum of the 2g-Mo appears broad (compare 2.3 ± 0.2 eV for synthesized materials *vs* 0.9 ± 0.03 eV for the reference sample) and the asymmetry suggests the presence of more than one species. Ozkar *et al*. reported molybdenum oxides located in the α-cages of sodium zeolite Y to have spectra broader than those of bulk MoO_3, with shift in BE from 232.7 eV for the bulk MoO_3 to BE ~233.6 eV for the MoO_3 encapsulated in sodium zeolite Y.[43] Therefore, even though unambiguous assignment of the molybdenum species in the 2g-Mo sample is difficult, based on similarity with the

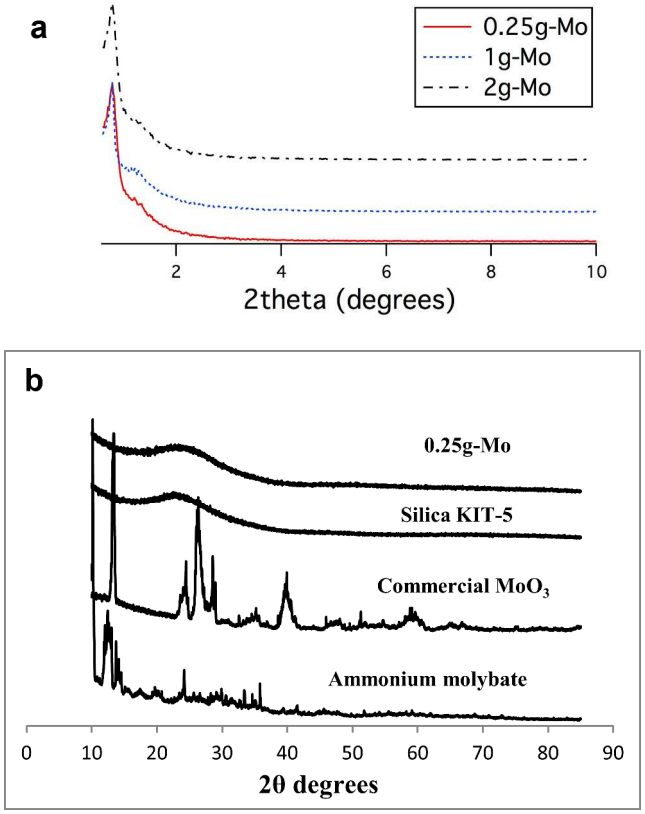

Figure 1: Low angle (a) and wide angle (b) X-ray diffraction patterns for the 0.25g-Mo catalyst, commercial molybdenum trioxide and the molybdenum precursor

n[MoO_3]-$Na_{56}Y$ system, we propose that the species at lower binding energy (~232.6 eV) are likely due to pure bulk MoO_3 and species located at higher binding energies (~233.8 eV and 234.6 eV) are due to encapsulated MoO_3 (molecular metal

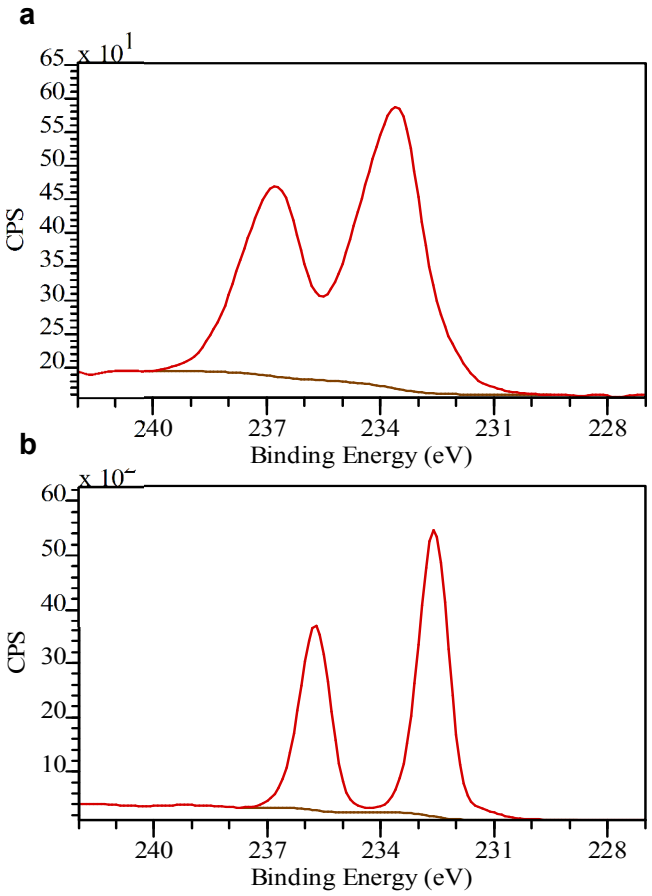

Figure 2: XPS high resolution Mo 3d spectra of 2g-Mo catalyst (a) and reference molybdenum trioxide (b)

oxides). Andersson *et al*. also reported molybdenum species at 233.7 eV, attributing them to an oxide layer forming over Mo(0) clusters.[44] The fact that most of the encapsulated MoO_3 is located at ~233.8 eV with smaller amount detected at ~234.6 eV suggest that there might be more than one site in the SiO_2 structure that anchors MoO_3 monomers or clusters. The increased line widths may also indicate different sized clusters.[44]

3.1.3 Physisorption and Chemisorption Analyses: Textural properties were attained by nitrogen physisorption analyses of the synthesized catalysts. The isotherms are shown in Figure 3, pore size distributions are illustrated in Figure S1, and the results are tabulated in Table 1. The specific surface areas of the 0.25g-Mo, 1g-Mo and 2g-Mo catalysts are 732, 690 and 685 m^2g^{-1}, respectively. The surface area of the catalyst decreased initially with an increase in molybdenum loading for 0.25g-Mo and 1g-Mo.

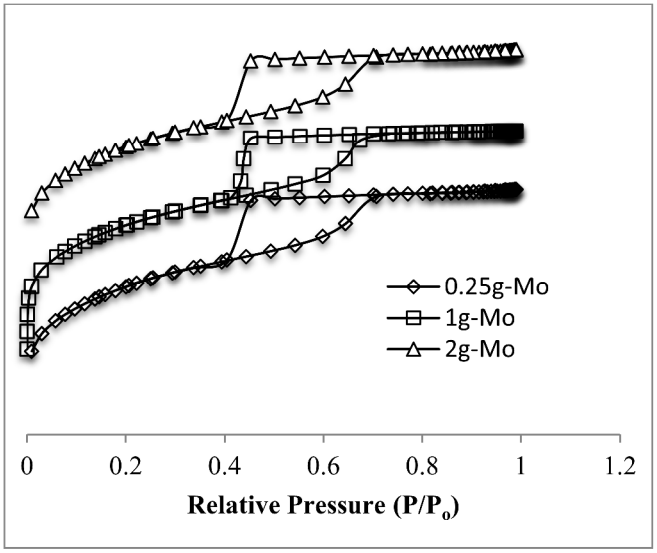

Figure 3: Nitrogen physisorption isotherms for the synthesized catalysts. The isotherms were offset on the y-axis for clarity.

When the molybdenum loading was increased from 2.5 to 3.7 wt% the decrease in surface area was negligible. The pore volumes of the catalyst decreased from 0.47 to 0.31 cm^3g^{-1} and the pore diameters of catalysts decreased from 6.2 nm to 4.3 nm with increasing molybdenum loading. All three catalysts exhibited type IV isotherms and type II hysteresis loops corresponding to mesoporous materials.[26] All three catalysts showed a steep increase in nitrogen adsorption around the relative pressure (P/P_o) of 0.4. Such a steep increase indicated a narrow and uniform pore size distribution within the catalyst. Furthermore, the hysteresis loops observed for the catalysts were characteristic of cage type materials such as KIT-5.[26]

The amount of acid sites present in the catalyst 0.25g-Mo, 1g-Mo and 2g-Mo were measured using ammonia TPD and total acid sites were found to be 55, 77, and 98 μmol g

[1], respectively and the results are summarized in Table S1. The desorption of ammonia molecules were determined to occur at approximately the same temperature for all the three catalysts (Figure S2). This indicates that the strength of the acid sites were similar regardless of molybdenum loading in the catalyst. Furthermore, the ammonia TPD profile suggests an abundance of a single type of acid strength on each of the catalysts. The relative quantities of Lewis and Brønsted acid sites in the catalysts were measured using pyridine DRIFTS. These measurements suggest that all the three catalysts have predominantly Lewis type acid sites and nearly negligible amount of Brønsted acid sites present in the catalyst.

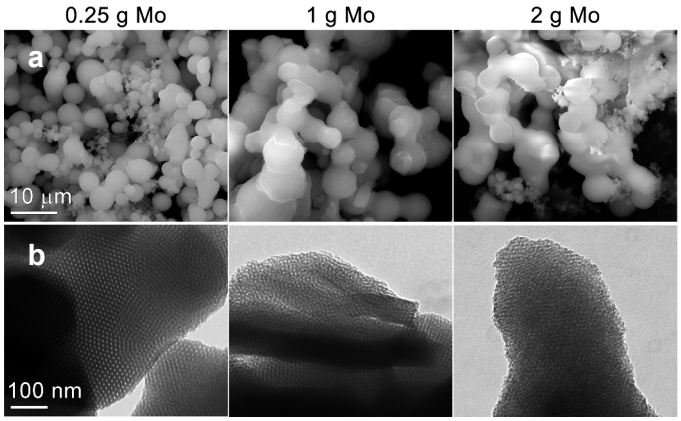

Figure 4: Scanning (**a**) and transmission (**b**) electron microscopy images of catalyst particles.

3.1.4 Electron Microscopy Analysis: The micro- and nano-scale morphology of the catalyst particles was investigated by SEM (Figure 4a) and TEM, (Figure 4b). The catalyst microstructure generally appeared as agglomerates of spherical particles with approximate diameters of ~1-5 μm and smaller, non-spherical particulates. The lower Mo loadings produced a dominant morphology of well-defined spheres, while higher Mo loadings produced structures that appeared as fusions of the spherical constituents. The characteristic face-centred cubic mesoporous nanostructure of the silica support fabricated using the previously mentioned F127 triblock copolymer is evident in the mesostructures clearly observed in the TEM micrographs shown in Figure 4b.[26] The porous network appears highly ordered at the lowest Mo loadings, and becomes increasingly disordered as the Mo loading increases.

Energy dispersive X-ray spectroscopy (EDS) was employed to investigate the elemental composition of the catalysts containing various Mo loadings. These results are presented in Table S2. The molybdenum loadings predicted from EDS analysis does not present a clear trend as we observed in ICP analysis (Table 1). The EDS analysis is capable of measuring molybdenum present on the surface of the catalyst support and cannot detect the molybdenum present inside the pores of the catalyst. The absence of the expected trend as in ICP analysis of the molybdenum loading suggests that the distribution of molybdenum on the surface and inside the pores varies from catalyst to catalyst (depending on Mo loading) or that the agglomeration of spherical particles as seen in Figure 4a impacts the surface oriented detection by EDS. The molybdenum dispersion was measured by EDS mapping of two catalyst samples (0.25g-Mo and 1g-Mo) (Figure 5 and Figure S3). These results show that the Mo is homogeneously dispersed throughout the surface of the silica support, and is not segregated or predominantly located with either particular morphology observed in the SEM micrographs.

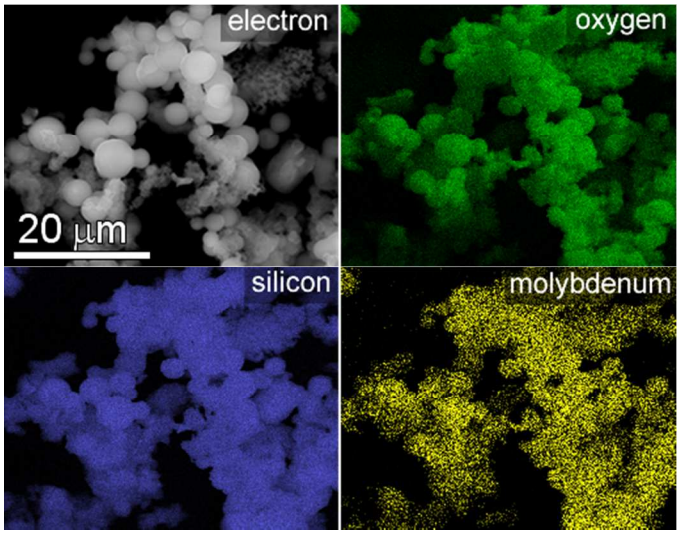

Figure 5: EDS mapping of 0.25g-Mo catalyst particles used to measure dispersion of active species within the catalysts.

3.2 Catalytic Fast Pyrolysis:

3.2.1 The mass spectra obtained from fast pyrolysis of cellulose, lignin and pine without catalyst are shown in Figure 6. The species in these spectra are composed of oxygenated products including aldehydes, ketones, carboxylic acids and phenolics along with hydrocarbons, water, carbon monoxide and carbon dioxide.[29] The oxygenated species give the resulting bio-oil several undesirable characteristics such as acidity, instability, and immiscibility with petroleum oil. Therefore, the pyrolysis products need to be upgraded to produce hydrocarbon intermediates or fuel blendstocks.[4, 45]

Catalytic fast pyrolysis (CFP) with zeolites upgrades biomass pyrolysis products to hydrocarbons,[29, 36, 46] however they suffer from low yields due to high light gas production and excessive catalyst coking.[47] The molybdenum catalyst explored here has low acidity as determined by ammonia TPD (Table S1) compared to zeolites, thus it will partially deoxygenate pyrolysis products and can potentially form less coke. This hypothesis was supported by a recent report from Mukarakate *et al*. where they found that catalysts containing high acidity produced completely deoxygenated species. Alternatively, catalyst having low acidity produced partially deoxygenated species such as furans, phenols and cresols.[36]

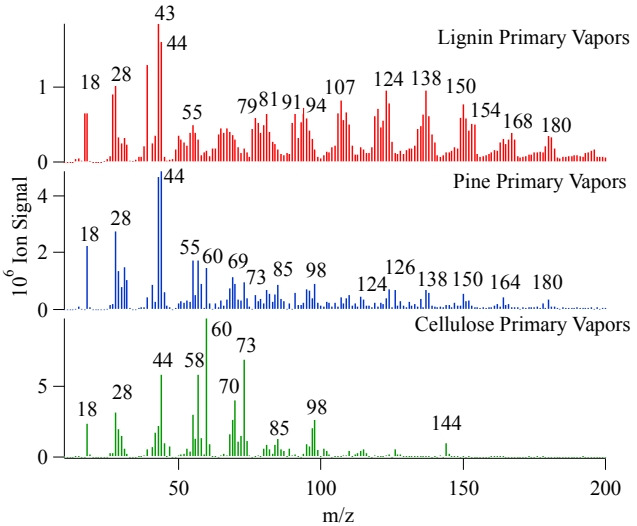

Figure 6: Mass spectra of pyrolysis products of cellulose (green), pine (blue), and lignin (red) at 500 °C obtained from an uncatalyzed, horizontal reactor-MBMS.

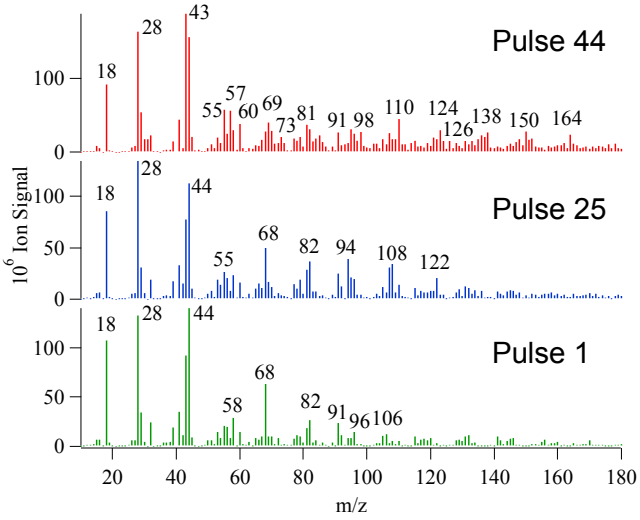

Figure 7: Mass spectra collected for pine pyrolysis vapors at different stages of catalytic upgrading demonstrating a changing pattern in evolution of compounds as the catalyst ages.

Figure 7 show mass spectra recorded at different points of the CFP experiment using 2g-Mo catalyst. In this experiment, sample holders containing 50 mg of pine were pyrolyzed sequentially over a fixed bed of 0.5 g of 2g-Mo catalyst. The pulses were fed continuously until the primary vapors of pine pyrolysis began to appear in the spectra. After the pyrolysis vapors of the first 50 mg of pine passed through the catalyst bed, a spectrum different from that of uncatalyzed pine pyrolysis (Figure 6) was obtained. As is also shown in py-GCMS analysis, the upgraded spectrum of pine consists of furan m/z 68, methyl furan m/z 82, dimethyl furan m/z 96, toluene m/z 92, xylenes m/z 106 and some light gases. The furan derivatives could be formed from upgrading the pyrolyzed carbohydrate components of pine while toluene and xylenes are predominantly upgraded vapors from the lignin component of pine. The spectrum recorded for pulse 44 is similar to uncatalyzed pine pyrolysis products (Figure 6) implying that the catalyst is completely deactivated at this point. However, the spectrum recorded for pulse 25 contains new peaks in addition to those observed for pulse 1, indicating partial deactivation of the catalyst. The new

species included phenol m/z 94, cresols m/z 108, and methyl cresols m/z 122. These species could be formed primarily from upgrading the lignin component of pine.[29]

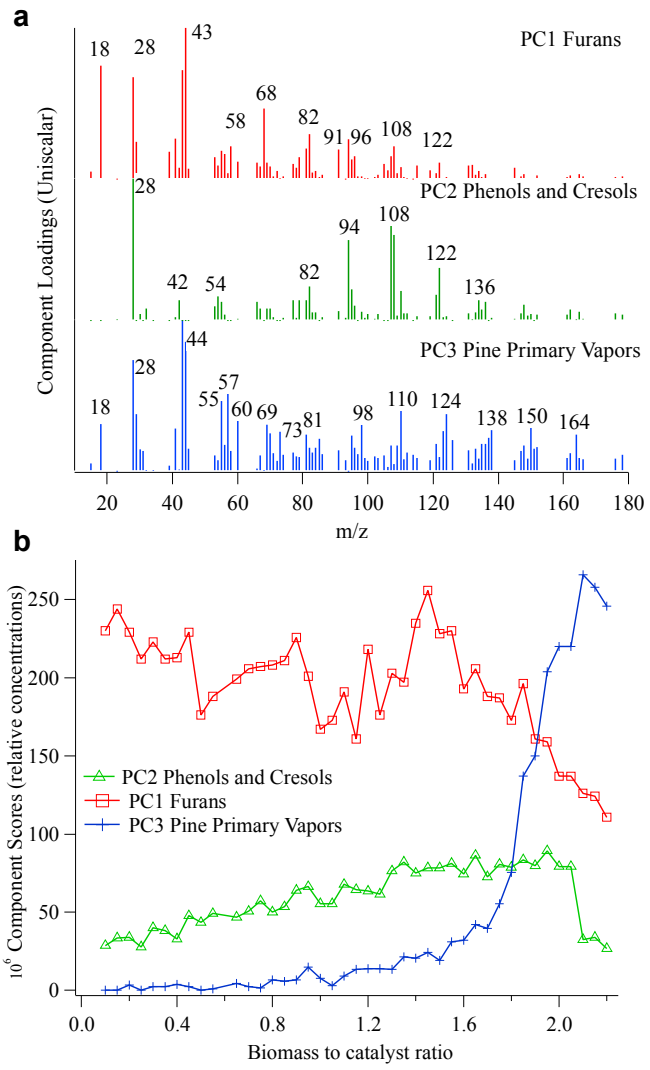

Figure 8: a) Reconstructed spectra (unit-vector normalized) from MCR-ALS analysis for each pure component (PC 1 through PC 3) of CFP of 44 pulses of pine pyrolysis vapors over 500 mg of catalyst 2g-Mo, enlightening changes in the composition of the product streams as the catalyst ages. b) Component scores plot from MCR-ALS analysis of CFP experiment illustrating the dependency of each PC on the biomass-to-catalyst ratio.

Since we obtained 44 spectra and each spectrum contains tens to hundreds of species, we use multivariate analysis to find trends in the data. Specifically, we are interested in exploring product changes as catalyst deactivates during the sequential pyrolysis of 44 pulses of pine biomass. We used the MCR-ALS approach, which has been used in previous studies to mathematically extract pure components from data sets with overlapping mass spectra obtained from catalytic upgrading of pine vapors using HZSM-5 catalyst.[29, 35, 36]

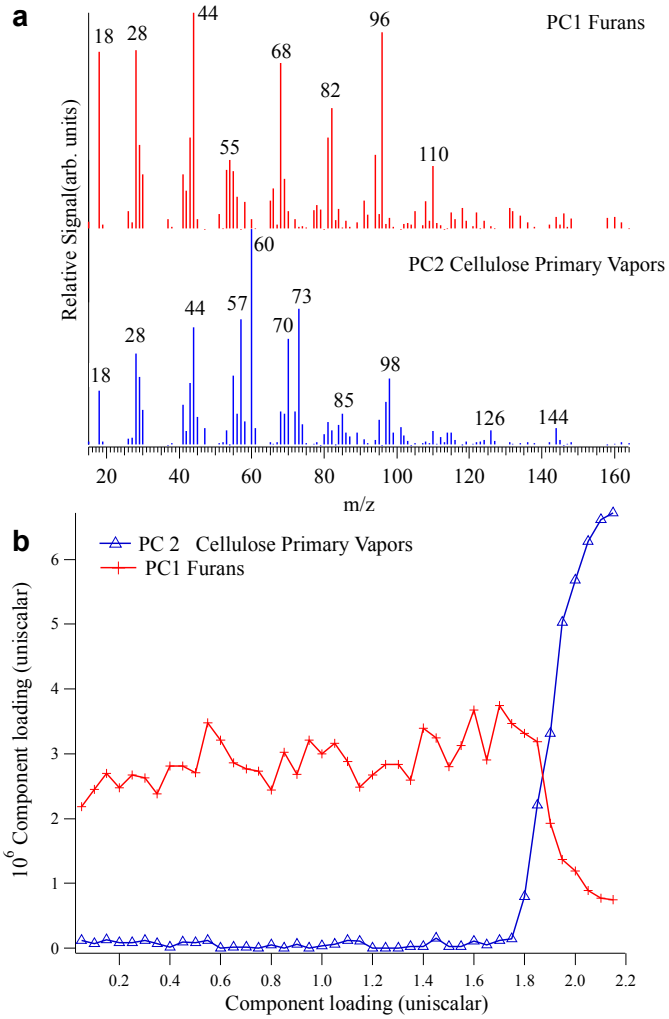

Figure 9: (a) Reconstructed spectra (unit-vector normalized) from MCR-ALS analysis for each pure component (PC1 & PC2) of CFP of 44 pulses of cellulose over 500 mg of catalyst 2g-Mo, enlightening changes in the composition of the product streams as the catalyst ages. (b) Component scores plot from MCR-ALS analysis of CFP experiment illustrating the dependency of each PC with biomass-to-catalyst ratio.

A data set prepared with dimensions of 44 pulses across the 100 product masses with largest variance was selected for this analysis. The MCR-ALS analysis was optimized for three pure components (PCs), which showed different catalyst

activity on upgrading biopolymers. The loadings for the three PCs are presented in Figure 8a. PC1 is approximately the same as the mass spectra derived for pulse 1. It contains intense furan and furan derivative peaks including furan m/z 68, methyl furan m/z 82, and dimethyl furan or furfural m/z 96. We hypothesize that these species are formed from the carbohydrate components of pine. Additionally, some low intensity peaks for phenol and cresols were also observed.

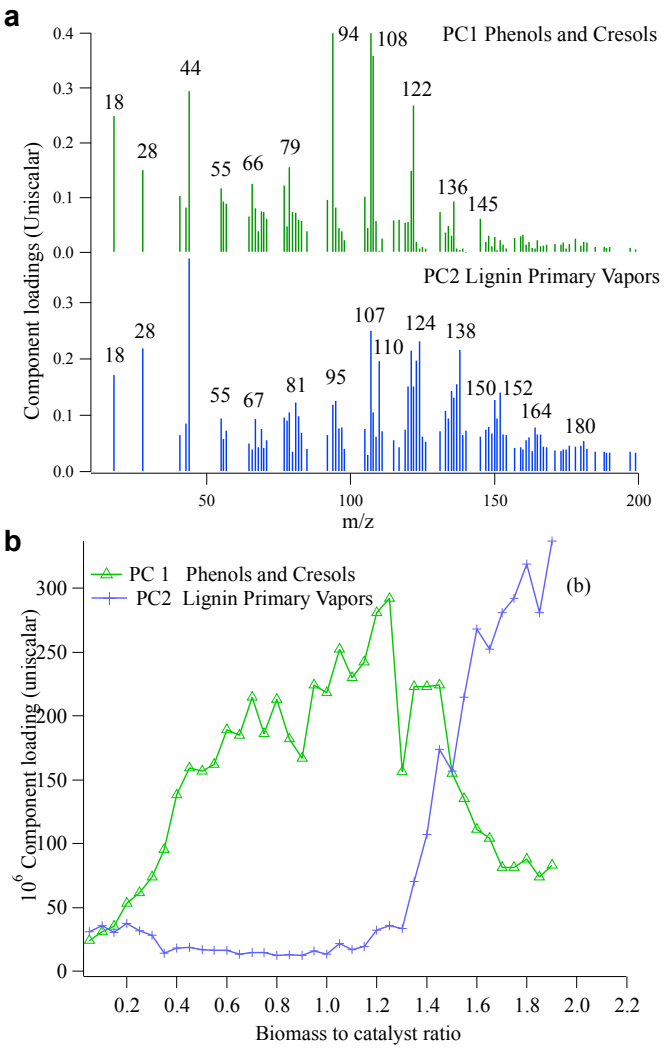

Figure 10: (a) Reconstructed spectra (unit-vector normalized) from MCR-ALS analysis for each pure component (PC1 and PC2) of CFP of 44 pulses of lignin over 500 mg of catalyst 2g-Mo, enlightening changes in the composition of the product streams as the catalyst ages. (b) Component scores plot from MCR-ALS analysis of CFP experiment illustrating the dependency of each PC with biomass-to-catalyst ratio.

These products are clearly enhanced in PC2. This PC contains phenol and phenol derivatives including phenol m/z 94, cresol m/z 108, methyl cresol m/z 122, and dimethyl cresols m/z 136. PC3 is very similar to the mass spectra obtained for pulse 44, which contains mostly primary vapors of pine pyrolysis.

The product distribution observed for molybdenum catalyst is different from observations of HZSM-5 made by Mukarakate *et al*.[29] This work studied the deactivation of HZSM-5 during fast pyrolysis of pine. For HZSM-5, the PC1 contains completely deoxygenated aromatic hydrocarbons, PC2 contains partially deoxygenated furans, phenols and cresols, and PC3 contains pine primary vapors.

The scores plot for the three PCs as a function of biomass-to-catalyst ratio (Figure 8b) exhibits the changing patterns of these molecules during deactivation of the catalyst. Furans were the major products (PC1), then as more biomass vapors pass through the bed, phenols and cresols (PC2) evolved as the dominant product over furans, and primary vapors of pine pyrolysis (PC3) are the major products towards the end due to catalyst deactivation. Furthermore, it was observed from the scores plot that the catalyst was fully active until a biomass-to-catalyst ratio of 1.5. Catalyst deactivation is typically attributed to deposition of carbonaceous species, commonly referred to as coke, on the catalyst. This coke is physisorbed on the surface and within the pores of the catalyst, covering the active catalytic sites and inhibiting further interaction of pyrolysis vapors with catalytic active sites.

3.2.2 CFP of Cellulose: Following the investigation of pine pyrolysis in the presence or absence of catalyst, we proceeded to investigate the individual biopolymers of pine (cellulose, hemicellulose and lignin) to explore the relation between the evolved products and the constituent biopolymers. Of the three biopolymers, we focused our work on cellulose to represent carbohydrates and lignin. Unlike the component loadings plot for pine, which has three PCs (PC1, PC2 and PC3) the loadings plot for cellulose contains only two PCs as

shown in Figure 9a. PC1 of cellulose contains predominantly furans (furan m/z 68, methylfuran m/z 82, dimethylfuran m/z 96 and trimethylfuran m/z 110). This agrees with our hypothesis that the furans were formed from the carbohydrate component of pine. The scores plot in Figure 9b shows that the catalyst was robust in producing furans until the biomass-to-catalyst ratio reached 1.8. After this point the catalyst became deactivated, furan formation dropped rapidly, and primary vapors for cellulose pyrolysis increased rapidly (PC2). Significant reports in the literature can be found for the production of furfural and 5-hydroxymethylfurfural (5-HMF) from cellulose or biomass, but no reports were found for production of furans exclusively from cellulose.[8-10, 12, 45] In our case, 5-HMF (m/z 126) and furfural (m/z 98) were observed during the fast pyrolysis of cellulose and pine in the absence of a catalyst along with other primary vapors. Mukarakate *et al.* reported the production of furans as intermediate products during the fast pyrolysis of cellulose using HZSM-5 catalyst.[29] During the fast pyrolysis of cellulose with HZSM-5 catalyst, completely deoxygenated aromatic hydrocarbons such as benzene, toluene, xylenes, indene, and naphthalenes were the major products before the onset of catalyst deactivation. Only at the onset of HZSM-5 deactivation, intermediate products were identified including furans, phenols and cresols. However, in the presence of Mo-catalyst, phenols and cresols were not as predominant as observed in HZSM-5 catalyzed pyrolysis.

3.2.3 CFP of Lignin: The component loadings plot for lignin is shown in Figure 10a. PC1 of lignin is composed of phenol and cresols, specifically phenol m/z 94, cresol m/z 108, methyl cresol m/z 122, and dimethyl cresol m/z 136. PC2 is composed of lignin primary pyrolysis products as shown in Figure 6.

The scores plot shown in Figure 10b reveals that phenol and cresols (PC1) form until a biomass-to-catalyst ratio of 1.3 was reached. Lignin primary vapors (PC2) begin to breakthrough at a biomass-to-catalyst ratio of 1.4 indicating that the catalyst is deactivated. Like cellulose, fast pyrolysis of lignin with HZSM-5 catalyst has produced aromatic hydrocarbons such as benzene, toluene, xylene and naphthalene as major products when the catalyst is fresh. These products were not observed with molybdenum catalyst as major products at any stage of catalyst reactivity. Once catalyst deactivation had started with HZSM-5, partially oxygenated species such as phenols and cresols evolved as intermediates.[29] In summary, fast pyrolysis of cellulose and lignin using molybdenum catalyst produced primarily partially oxygenated species such as furans, phenols and cresols as the major products when the catalyst is fully active. These same products were identified only as intermediates with HZSM-5 catalyst coinciding with the onset of deactivation.

After the investigation of CFP of biopolymers lignin and cellulose, we concluded that the catalyst deactivates more slowly with cellulose than with lignin as evidenced by the biomass-to-catalyst ratios of 1.8 and 1.4, respectively. Even though the difference in biomass-to-catalyst ratio appears small, when we consider the weight percentage of primary vapors that pass through the catalyst, they are significantly different. The weight percentage of char measured for cellulose and lignin are 3.4 and 33 wt%, respectively. These values are in agreement with values reported by Mukarakate *et al.*[29] This indicates that cellulose is producing 30 wt % more primary pyrolysis vapors than lignin, yet despite this huge difference in primary vapor production, the catalyst deactivates at a higher biomass-to-catalyst ratio for cellulose than lignin. Thus, the catalyst is losing its activity to the lignin component of pine faster than cellulose. Interestingly, the biomass-to-catalyst ratios for catalyst deactivation of pine and cellulose are nearly the same at 1.7 and 1.8, respectively. This suggests that the lignin component in the pine is not deactivating the catalyst to the same extent as it does as an independent fuel. This can be attributed to the fact that the majority of pine is carbohydrate (65%) and the balance is lignin.

3.2.4 Effect of molybdenum loading on deactivation: Figure 11, summarizes the activity of catalysts containing different loadings of molybdenum towards fast pyrolysis of cellulose, lignin and pine. 0.25g-Mo, 1g-Mo and 2g-Mo catalysts were investigated for cellulose fast pyrolysis, and their biomass-to-catalyst ratios for deactivation were found to be 0.55, 1.3 and 1.8, respectively. To appreciate the difference in activity of the catalysts, and the specific activity of catalysts towards cellulose, lignin and pine, we have replaced the biomass-to-catalyst ratio term with biomass vapors-to-catalyst ratio. The amount of primary vapors produced per unit weight for the pine, cellulose and lignin are quite different and measured based on the char weight percentage (cellulose 3.4 wt%, lignin 33 wt% and pine 17.8 wt%). Thus, we translated the biomass-to-catalyst ratio of 0.55, 1.3, and 1.8 as biomass vapors-to-catalyst ratio 0.53, 1.26 and 1.74, respectively. The biomass vapors-to-catalyst ratio increased with increasing molybdenum loading in the catalyst. When normalized for molybdenum loading on each catalyst, the biomass vapors-to-catalyst ratios decreased for 0.25g-Mo, 1g-Mo and 2g-Mo catalysts to 0.25, 0.5 and 0.5, respectively. These values suggest that 0.25g-Mo is the least efficient at upgrading, while 1g-Mo and 2g-Mo were equally efficient. This observation suggests that the active sites in the 1g-Mo and 2g-Mo catalysts were equally accessible to the pyrolysis vapors. This is also indicative of a lack of molybdenum agglomeration or sintering during the synthesis and during the reaction progress for 1g-Mo and 2g-Mo. The poor efficiency of 0.25g-Mo requires further investigation. The biomass vapors-to-catalyst ratio of 2g-Mo catalyst for lignin and pine were observed to be 0.88 and 1.4, respectively; indicating that lignin is the most resistant biopolymer to convert to desired products. The biomass vapors-to-catalyst ratio for pine (1.4) is lower in comparison to cellulose (1.74), which can be attributed to presence of lignin in pine.

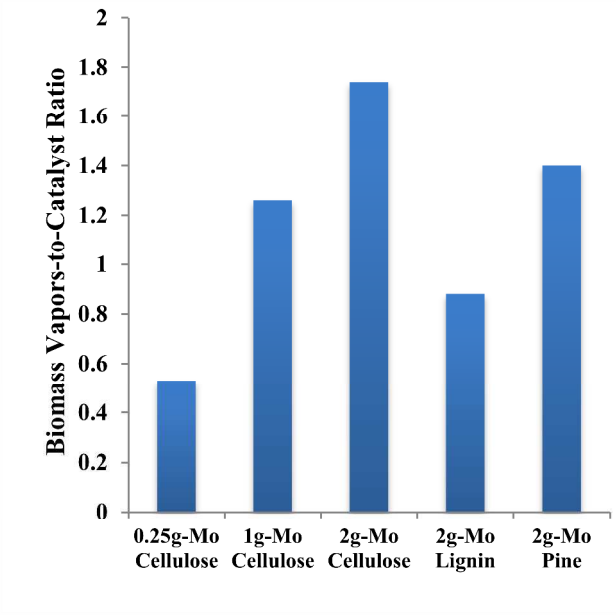

Figure 11. Summary of biomass-to-catalyst ratios for deactivation of catalysts with different molybdenum loading reacting with the pyrolysis vapors from biopolymers and pine.

3.2.5 Quantification of Pyrolysis Products: To identify the specific products and complement the results obtained from MBMS analysis, py-GCMS experiments were carried out and yields for some of the major products were measured at a biomass-to-catalyst ratio of 0.1. The list of products identified is presented in Table S3. As observed in py-MBMS, the major products (furans, light gases, phenols and aromatics) were identified from this experiment. Along with those compounds, olefins such as cyclobutene, cyclopentenes, cyclopentadienes, and carbonyl compounds such as propenals, and butenones were also identified.

Of the several products that were identified by py-GCMS we were able to calculate the yields for some furans (furan, 2-methylfuran, 2,5-dimethylfuran), some phenols (phenol and *m*-cresol), and some aromatics (benzene, toluene, and *p*-xylene) for all three catalysts. In all three catalysts, furans were identified as the major products (~ 1 wt % of biomass) and molybdenum loading does not influence the distribution of products. Phenols and aromatics were found to be 0.1 wt % for all three catalysts. Aromatics were found to be 0.04 wt % for 0.25g-Mo and 1g-Mo while it is 0.08 wt % for 2g-Mo

catalyst. Summary of this findings are presented in Table 2.

Table 2: Summary of weight percent of major products identified during fast pyrolysis of pine using different catalysts.

Catalyst	Furans[a] (wt %)	Aromatic[b] (wt %)	Phenols[c] (wt %)
0.25g-Mo	1.05	0.04	0.1
1g-Mo	0.96	0.04	0.1
2g-Mo	1.3	0.08	0.1

[a]Furan, 2-methylfuran, and 2,5-dimethylfuran; [b]phenol and *m*-cresol; [c]benzene, toluene and *p*-xylene.

3.2.6 Coke Analysis: TGA analysis was performed to evaluate the amount of coke built up on the catalyst. 2g-Mo catalyst was subjected to pine fast pyrolysis vapors and removed from the reactor at the biomass-to-catalyst ratio of 1.4 where the onset of catalyst deactivation was observed. Similarly, the catalyst samples subjected to fast pyrolysis of cellulose and lignin were removed from the reactor at the biomass-to-catalyst ratio of 1.74 and 0.88, respectively. The amount of coke was determined by heating the sample in air to 780 °C and measuring the mass loss as shown in Figure 12. The mass loss below 250 °C (6.3%) was attributed to moisture and weakly adsorbed organic species, which is in agreement with previous reports.[27] Analysis of a fresh catalyst showed significant mass loss (13%) below 250 °C and confirmed that the mass loss below 250 °C was not due to coke. The mass loss for pine, cellulose and lignin are 16.9 wt%, 18.5 wt% and 14.5 wt% (on a coke and moisture-free basis), respectively. The mass loss that occurred between 250 °C and 650 °C was attributed to coke deposited on the catalyst. From the char wt% calculated for cellulose (3.4 wt%), lignin (33 wt %) and pine (17.8 wt%), it is evident that cellulose produced significantly more pyrolysis vapors than lignin or pine and hence more coke was deposited on the catalyst from fast pyrolysis of cellulose and the least amount of coke was measured for lignin. Normalization of coke deposited on catalyst to amount of biomass required for the onset of deactivation of catalyst for fast pyrolysis of pine, cellulose and lignin was measured as 8.6, 8.9 and 9.9 wt%, respectively. These normalized results show that lignin forms more coke, which supports the low biomass vapors-to-catalyst ratio for deactivation in comparison to pine and cellulose.

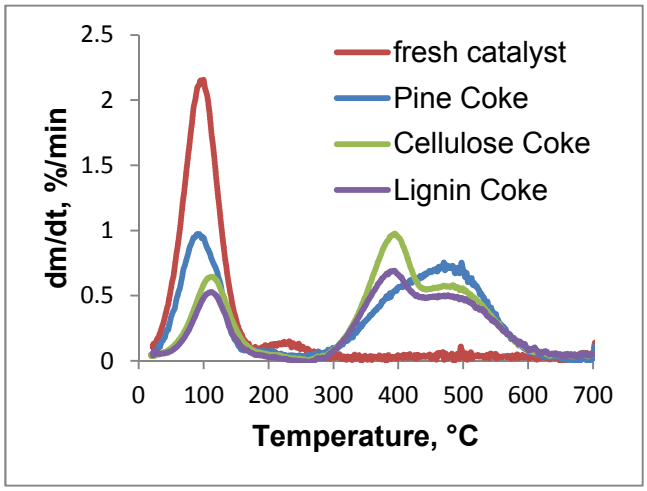

Figure 12. Effect of temperature on combustion of coke deposited on 2g-Mo catalyst retrieved at the onset of deactivation for fast pyrolysis of pine.

4. Conclusions

Catalysts with different loadings of molybdenum on KIT-5 mesoporous silica support were synthesized by a co-condensation method. Characterization studies indicated that the incorporated molybdenum was in a trioxide form and homogeneously distributed over the catalyst. When the catalyst was subjected to fast pyrolysis vapors from pine or biopolymer cellulose it was highly selective for the production of furans, a valuable jet/diesel fuel precursor. Catalysts 1g-Mo and 2g-Mo performed better than 0.25g-Mo towards biomass conversion. Lignin formed more coke on the catalyst (g coke/g biomass) leading to rapid catalyst deactivation. The influence of pore-size and pore structure on catalytic activity and strategies to improve the yield of furans with this catalyst are currently under investigation.

Acknowledgements

This work was supported by U.S. Department of Energy's Bioenergy Technologies Office (DOE-BETO) under contract No. DE-AC36-08GO28308 with the National Renewable Energy Laboratory. Also BGT and SB would like to thank the Colorado School of Mines for support of this project. Thanks to Daniel Carpenter for support with MBMS experiments.

Notes and references

[a]National Renewable Energy Laboratory, 15523 Denver West Parkway, Golden, CO 80401-3393. Email: Calvin.Mukarakate@nrel.gov

[b]Colorado School of Mines, Department of Chemistry and Geochemistry, 1012 14th Street, Golden, CO 80401-3393. Email: btrewyn@mines.edu

Electronic Supplementary Information (ESI) available: [details of any supplementary information available should be included here]. See DOI: 10.1039/b000000x/

1. P. Gallezot, *Chemical Society Reviews*, 2012, 41, 1538-1558.
2. A. Corma, S. Iborra and A. Velty, *Chem Rev*, 2007, 107, 2411-2502.
3. T. Werpy, G. Petersen, A. Aden, J. Bozell, J. Holladay, J. White, A. Manheim, D. Elliot, L. Lasure, S. Jones, M. Gerber, K. Ibsen, L. Lumberg and S. Kelley, *Top Value Added Chemicals from Biomass Volume 1 - Results of Screening for Potential Candidates from Sugars and Synthesis Gas*, Office of Biomass Programm, 2004.
4. A. D. Sutton, F. D. Waldie, R. Wu, M. Schlaf, L. A. Pete' Silks, III and J. C. Gordon, *Nat. Chem.*, 2013, 5, 428-432.
5. A. Gandini and N. M. Belgacem, *Polym. Int.*, 1998, 47, 267-276.
6. K. T. Hopkins, W. D. Wilson, B. C. Bender, D. R. McCurdy, J. E. Hall, R. R. Tidwell, A. Kumar, M. Bajic and D. W. Boykin, *J. Med. Chem.*, 1998, 41, 3872-3878.
7. D. T. Richter and T. D. Lash, *Tetrahedron Lett.*, 1999, 40, 6735-6738.
8. C. Moreau, A. Finiels and L. Vanoye, *J. Mol. Catal. A: Chem.*, 2006, 253, 165-169.
9. Y. Roman-Leshkov, J. N. Chheda and J. A. Dumesic, *Science (Washington, DC, U. S.)*, 2006, 312, 1933-1937.
10. J. N. Chheda, Y. Roman-Leshkov and J. A. Dumesic, *Green Chem.*, 2007, 9, 342-350.
11. H. Zhao, J. E. Holladay, H. Brown and Z. C. Zhang, *Science (Washington, DC, U. S.)*, 2007, 316, 1597-1600.
12. F. L. Yang, Q. S. Liu, X. F. Bai and Y. G. Du, *Bioresource Technol*, 2011, 102, 3424-3429.
13. H. Ishida and K.-i. Seri, *J. Mol. Catal. A: Chem.*, 1996, 112, L163-L165.
14. S. Dutta, S. De, A. K. Patra, M. Sasidharan, A. Bhaumik and B. Saha, *Applied Catalysis, A: General*, 2011, 409-410, 133-139.
15. X. Guo, Q. Cao, Y. Jiang, J. Guan, X. Wang and X. Mu, *Carbohydrate Research*, 2012, 351, 35-41.
16. I. J. Kuo, N. Suzuki, Y. Yamauchi and K. C. W. Wu, *RSC Advances*, 2013, 3, 2028-2034.
17. Y.-C. Lee, S. Dutta and K. C. W. Wu, *ChemSusChem*, 2014, 7, 3241-3246.
18. X. Tong, Y. Ma and Y. Li, *Appl. Catal., A*, 2010, 385, 1-13.
19. D. Zhao, S. Budhi, A. Rodriguez and R. T. Koodali, *Int. J. Hydrogen Energy*, 2010, 35, 5276-5283.
20. S. Budhi, H. S. Kibombo, D. Zhao, A. Gonshorowski and R. T. Koodali, *Mater. Lett.*, 2011, 65, 2136-2138.
21. C. T. Kresge, M. E. Leonowicz, W. J. Roth, J. C. Vartuli and J. S. Beck, *Nature*, 1992, 359, 710-712.
22. J. Y. Ying, C. P. Mehnert and M. S. Wong, *Angew Chem Int Edit*, 1999, 38, 56-77.
23. Y. Wan and D. Y. Zhao, *Chem Rev*, 2007, 107, 2821-2860.
24. H. Subramanian, E. G. Nettleton, S. Budhi and R. T. Koodali, *Journal of Molecular Catalysis A: Chemical*, 2010, 330, 66-72.
25. K. Lee, Y.-H. Kim, S. B. Han, H. Kang, S. Park, W. S. Seo, J. T. Park, B. Kim and S. Chang, *J. Am. Chem. Soc.*, 2003, 125, 6844-6845.
26. F. Kleitz, D. Liu, G. M. Anilkumar, I.-S. Park, L. A. Solovyov, A. N. Shmakov and R. Ryoo, *J. Phys. Chem. B*, 2003, 107, 14296-14300.
27. S. T. Oyama, *Journal of Catalysis*, 2003, 216, 343-352.
28. S. Budhi, C. Peeraphatdit, S. Pylypenko, V. H. T. Nguyen, E. A. Smith and B. G. Trewyn, *Appl. Catal., A*, 2014, 475, 469-476.
29. C. Mukarakate, X. Zhang, A. R. Stanton, D. J. Robichaud, P. N. Ciesielski, K. Malhotra, B. S. Donohoe, E. Gjersing, R. J. Evans, D. S. Heroux, R. Richards, K. Iisa and M. R. Nimlos, *Green Chem.*, 2014, 16, 1444-1461.
30. R. Chakravarti, H. Oveisi, P. Kalita, R. R. Pal, S. B. Halligudi, M. L. Kantam and A. Vinu, *Microporous Mesoporous Mater.*, 2009, 123, 338-344.
31. C. A. Emeis, *J. Catal.*, 1993, 141, 347-354.
32. S. M. Maier, A. Jentys and J. A. Lercher, *J. Phys. Chem. C.*, 2011, 115, 8005-8013.
33. R. J. Evans and T. A. Milne, *Energy Fuels*, 1987, 1, 311-319.
34. R. J. Evans and T. A. Milne, *Energy Fuels*, 1987, 1, 123-137.
35. R. French and S. Czernik, *Fuel Process Technol*, 2010, 91, 25-32.
36. C. Mukarakate, M. J. Watson, J. ten Dam, X. Baucherel, S. Budhi, M. M. Yung, H. Ben, K. Iisa, R. M. Baldwin and M. R. Nimlos, *Green Chem*, 2014, DOI: 10.1039/c4gc01425a.
37. E. R. Malinowski, *Abstr Pap Am Chem S*, 1986, 191, 194-CHED.
38. X. B. Ma, J. L. Gong, S. P. Wang, N. Gao, D. L. Wang, X. Yang and F. He, *Catal Commun*, 2004, 5, 101-106.
39. W. Gruenert, A. Y. Stakheev, R. Feldhaus, K. Anders, E. S. Shpiro and K. M. Minachev, *J. Phys. Chem.*, 1991, 95, 1323-1328.
40. S. S. Al-Shihry and S. A. Halawy, *J. Mol. Catal. A: Chem.*, 1996, 113, 479-487.
41. J. Zou and G. L. Schrader, *J. Catal.*, 1996, 161, 667-686.
42. D. S. Zingg, L. E. Makovsky, R. E. Tischer, F. R. Brown and D. M. Hercules, *J. Phys. Chem.*, 1980, 84, 2898-2906.
43. S. Ozkar, G. A. Ozin and R. A. Prokopowicz, *Chem Mater*, 1992, 4, 1380-1388.
44. S. L. T. Andersson and R. F. Howe, *J Phys Chem-Us*, 1989, 93, 4913-4920.
45. S. Dutta, S. De and B. Saha, *Biomass Bioenerg*, 2013, 55, 355-369.
46. A. V. Bridgwater, *Biomass Bioenergy*, 2012, 38, 68-94.
47. P. T. Williams and N. Nugranad, *Energy*, 2000, 25, 493-513.

TOC: